

# A dual-responsive polydopamine-modified hydroxybutyl chitosan hydrogel for sequential regulation of bone regeneration

Zhuqing Wan, Qinyuan Dong, Xiaodong Guo, Xiaoqiang Bai, Xiao Zhang, Ping Zhang, Yunsong Liu, Longwei Lv<sup>\*</sup>, Yongsheng Zhou<sup>\*</sup>

Department of Prosthodontics, Peking University School and Hospital of Stomatology, 22 Zhongguancun Avenue South, Haidian District, Beijing 100081, PR China

National Center of Stomatology, 22 Zhongguancun Avenue South, Haidian District, Beijing 100081, PR China

National Clinical Research Center for Oral Diseases, 22 Zhongguancun Avenue South, Haidian District, Beijing 100081, PR China

National Engineering Research Center of Oral Biomaterials and Digital Medical Devices, 22 Zhongguancun Avenue South, Haidian District, Beijing 100081, PR China  
Beijing Key Laboratory of Digital Stomatology, 22 Zhongguancun Avenue South, Haidian District, Beijing 100081, PR China

## ARTICLE INFO

### Keywords:

Anti-inflammation  
Bone regeneration  
Hydroxybutyl chitosan  
Near-infrared light  
Polydopamine  
Sequential delivery

## ABSTRACT

Delayed inflammatory reaction and poor osteogenesis are the two main causes of failure for bone-defect healing. Accordingly, in the present study, a dual-responsive hydrogel composite was successfully fabricated in which near-infrared (NIR)-light-responsive polydopamine-coated magnesium-calcium carbonate microspheres are incorporated into a thermo-responsive hydroxybutyl chitosan hydrogel to provide sequential delivery of the anti-inflammatory drug aspirin and osteogenic bone morphogenetic protein 2 (BMP-2). By initially releasing aspirin rapidly, the hydrogel composite efficiently ameliorates early-stage inflammatory reaction and promotes transition to the regenerative phase. Then, the hydrogel composite allows NIR-light-responsive release of BMP-2, which maximizes its osteoinductive effects. Using an SD rat calvaria-defect model, the sequential and controllable release achieved by the hydrogel is demonstrated to promote new-bone formation. Thus, the current study provides an efficient alternative strategy for developing multifunctional therapeutic biomaterials for bone tissue engineering.

## 1. Introduction

Bone defects caused by trauma, cancer, or infections leave many patients in pain and with disabilities, thus constituting a common clinical challenge (Liu et al., 2021). Many efforts have been made to fabricate three-dimensional (3D) scaffolds with appropriate architecture and osteoconductive capability, alone or functionalized with bioactive factors for enhanced bone regeneration (Cui et al., 2020; Zhao et al., 2020; Zhu et al., 2021). Natural bone-defect repair involves a cascade of biological events including early hemostasis and acute inflammatory response, mineralization, and bone remodeling (Annamalai et al., 2018; Claes et al., 2012). Acute inflammation is initiated by exogenous invasion and/or endogenous response (Zhang et al., 2021). Thereafter, the acute inflammatory phase transforms into the regenerative phase under the action of multiple signaling biomolecules (Italiani & Boraschi, 2014; Murray & Wynn, 2011). It has been demonstrated that osteoinductive signals are maximally efficient when applied during the late

inflammatory phase preceding the bone-repair stage, making it an optimal therapeutic biowindow for the delivery of osteogenic biomolecules (Einhorn & Gerstenfeld, 2015). Conversely, dysregulated inflammation disrupts the mineralization of the extracellular matrix and can even lead to irreversible bone resorption (Loi et al., 2016; Zhang et al., 2017). Accordingly, desired bone-tissue regeneration requires the amelioration of aberrant immune response and regulation of the therapeutic application of osteogenic biomolecules (Claes et al., 2012).

Among the currently available biomaterials used for bone-tissue regeneration, micro/nanoparticle-based hydrogel composites are particularly valuable owing to their design flexibility and drug-loading capability (Jalili et al., 2016; Lienemann et al., 2020). However, the biomolecule-release profiles of current hydrogel platforms are mostly dependent on their crosslinking densities and intrinsic biodegradation properties, making it difficult to modulate the therapeutic delivery of biomolecules in accordance with the requirements of bone regeneration (Kim & Tabata, 2015; Rothe et al., 2020; Zhu et al., 2020).

<sup>\*</sup> Corresponding authors at: Department of Prosthodontics, Peking University School and Hospital of Stomatology, 22 Zhongguancun Avenue South, Haidian District, Beijing 100081, PR China.

E-mail addresses: [lvlw@bjmu.edu.cn](mailto:lvlw@bjmu.edu.cn) (L. Lv), [kqzhouysh@hsc.pku.edu.cn](mailto:kqzhouysh@hsc.pku.edu.cn) (Y. Zhou).

<https://doi.org/10.1016/j.carbpol.2022.120027>

Received 11 May 2022; Received in revised form 18 August 2022; Accepted 22 August 2022

Available online 27 August 2022

0144-8617/© 2022 Published by Elsevier Ltd.

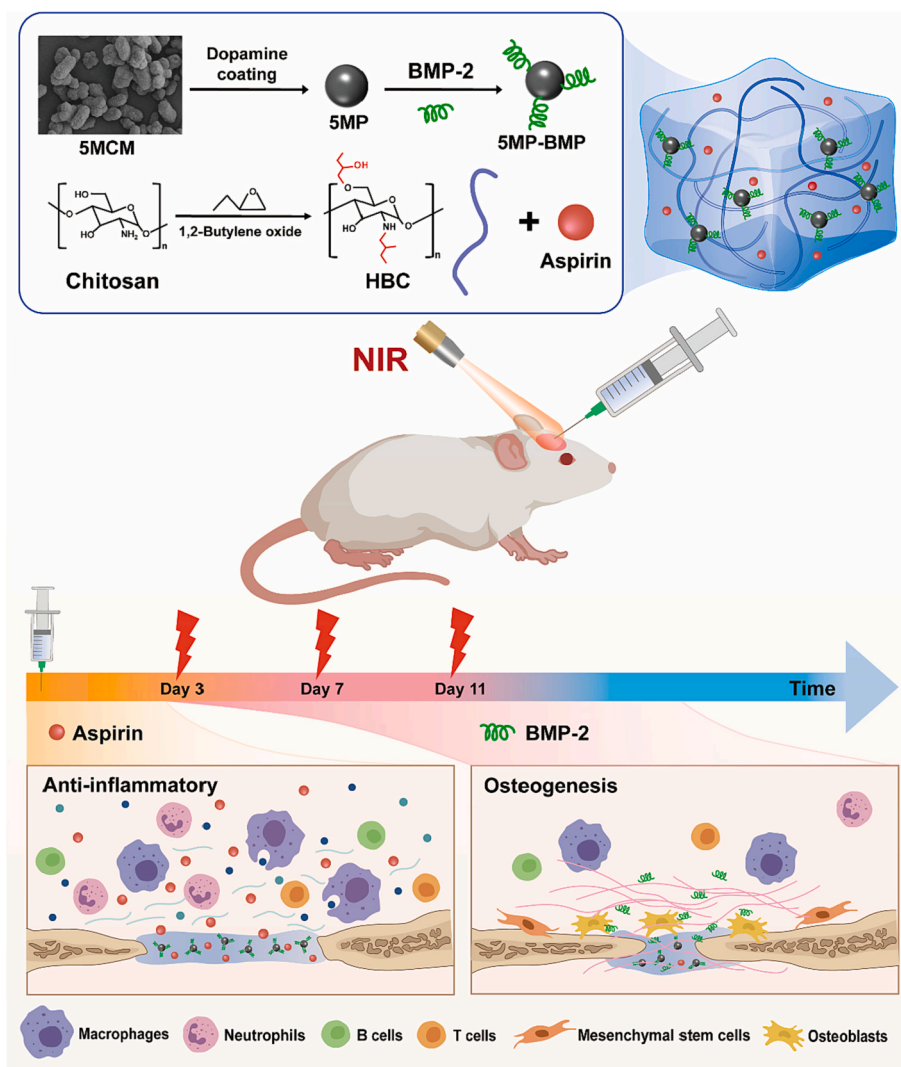


**Fig. 1.** Synthesis of the dual-responsive hydrogel composite by incorporating NIR-light-responsive PDA-coated magnesium-calcium carbonate microspheres into a thermo-responsive HBC hydrogel and its application for sequential Asp/BMP-2 delivery and *in situ* calvaria bone regeneration.

Hydroxybutyl chitosan (HBC) hydrogel, a temperature-responsive chitosan derivative, exhibits numerous merits, such as desirable water solubility, fast and reversible gelation, and excellent biocompatibility, making it a reliable option for establishing drug-delivery systems (Bi et al., 2021; Sun et al., 2020). Additionally, near-infrared (NIR)-light-responsive drug carriers exhibit superior versatility owing to the high tissue transparency of NIR light and its ability to be accurately controlled externally (Gao et al., 2019; Tong et al., 2019; Wan et al., 2020). Polydopamine (PDA) is an NIR-light-sensitive agent with versatile adhesive properties, excellent photothermal conversion capability, and efficient drug-loading and -release abilities (Liu et al., 2014). Thus, inorganic microspheres modified with a PDA coating could potentially serve as NIR-light-responsive drug carriers that are capable of controlled release. Therefore, the integration of PDA-based inorganic microspheres into HBC hydrogel may provide a means to achieve the sequential release of different biomolecules during bone healing.

Bone morphogenetic protein 2 (BMP-2) is an efficient bone-forming growth factor that is widely used as an exogenous biomolecule in bone regeneration (Moncal et al., 2022). In this study, PDA-coated magnesium-calcium carbonate microspheres were used as NIR-light-responsive carriers to regulate the therapeutic timeline of BMP-2, while HBC hydrogel was applied to deliver the anti-inflammatory drug aspirin (Asp) and relieve undesirable inflammatory response. It can be

hypothesized that this dual-responsive hydrogel-microsphere composite would effectively modulate the process of bone healing by the initial rapid release of Asp (first three days) and optimizing the release profile of BMP-2 under the control of NIR light in the later stage (3–14 days). Firstly, the thermo- and NIR-light-responsive properties of our hydrogel composite were examined. Then, the of Asp- and BMP-2-release profiles as well as the biodegradability of the hydrogel composite were evaluated. *In vitro* experiments were performed to examine the biocompatibility and osteogenic ability of the hydrogel composite. Finally, the *in situ* tissue response and osteogenesis capability of the hydrogel composite were investigated using an SD rat calvaria-defect model to evaluate the effects of this sequential release strategy on bone regeneration (Fig. 1).

## 2. Materials and methods

### 2.1. Synthesis and characterization of HBC

The HBC was prepared using a previously reported method (Wan et al., 2022). Briefly, 1 g chitosan (Mw = 190–375 kDa, DD ≥ 75 %, Sigma-Aldrich, USA) was alkalized in 20 mL NaOH (50 % w/w) at room temperature for 48 h. Then, the alkalized chitosan was dispersed in 20 mL isopropanol/water (1/1, v/v) for 24 h. Subsequently, 20 mL

1,2-butene oxide (Aladdin, China) was added dropwise and the mixture was reacted at 55 °C for another 72 h. The HBC product was neutralized with 0.1 M HCl, dialyzed against distilled water, freeze-dried, and sterilized under UV light. The elemental composition of the product was determined using an Vario EL-III elemental analyzer (Elementar, Germany). <sup>1</sup>H nuclear magnetic resonance (NMR) spectra were obtained in 20 % deuterated hydrochloric acid (DCl) using an Ultrashield 600 PLUS spectrometer (Bruker, Germany). Fourier transform infrared (FTIR) spectra were recorded using the KBr-pellet method on a Nexus470 FTIR spectrophotometer (Nicolet, USA) within the wavenumber range 4000–400 cm<sup>-1</sup> at a resolution of 4 cm<sup>-1</sup>.

## 2.2. Preparation of hydrogel-microsphere composites

BMP-2-loaded and PDA-modified 5 wt% magnesium containing calcium carbonate microspheres (5MP-BMP) were prepared according to the method detailed in the *Supporting Information*. Then, hydrogel-microsphere composites were fabricated according to Table S2. Taking the HBC+Asp+5MP-BMP hydrogel composite as an example, the 5MP-BMP microspheres were resuspended in 200 µg/mL Asp (Sigma-Aldrich, USA) solution. Then, the sterilized HBC was dispersed in the microspheres/Asp solution and stored at 4 °C for further dissolution.

## 2.3. In vitro release profiles

Typically, 200 µL HBC+Asp/HBC+Asp+5MP-BMP hydrogels were injected into each well of a 12-well plate. Then, 1 mL PBS solution was added to each well and the plate was incubated at 37 °C under 5 % CO<sub>2</sub>. Thereafter, 100 µL of the supernatant from each sample was collected and replaced with the same volume of fresh PBS at different time periods of incubation. The concentration of Asp in the supernatant was determined according to Lambert-Beer's Law by measuring its optical density at 296 nm using a Cary 60 UV spectrophotometer (Agilent, Singapore).

To evaluate the release profile of BMP-2, HBC+Asp+5MP-BMP hydrogel was injected into the upper chamber of a 24-well Transwell plate (0.4 µm, Corning, USA) and immersed into α-MEM culture medium for incubation. NIR light irradiation (0.25 W/cm<sup>2</sup>, 10 min) was performed on days 3, 7, and 11 and the concentrations of BMP-2 (*n* = 3) were determined on days 1, 2, 3, 5, 7, 9, 11, and 14 using BMP-2 enzyme linked immunosorbent assay (ELISA) kits (RayBiotech, USA).

## 2.4. Cell culture and cell viability assay

Primary human bone marrow-derived mesenchymal stem cells (hBMSCs; ScienCell, USA) were used for *in vitro* studies. Cells were cultured with proliferation medium (PM) containing α-MEM, 10 % fetal bovine serum, and 1 % antibiotics at 37 °C under 5 % CO<sub>2</sub> atmosphere.

First, *in vitro* cell viability was investigated by CCK-8 assay. The hBMSCs were seeded on the surfaces of hydrogel layers at a density of 1 × 10<sup>4</sup> cells/mL. The blank group was cultured without any hydrogel. After 1, 3, 5, and 7 days of culture, the cells in the HBC+5MP-BMP+NIR/HBC+Asp+5MP-BMP+NIR groups were irradiated under NIR laser (0.25 W/cm<sup>2</sup>, 10 min). Then, CCK-8 reagent (NCM Biotech, China) was added and the samples were incubated at 37 °C for 2 h. Quantification was performed by measuring the optical density of the supernatant at 450 nm.

Additionally, cell adhesion to the hydrogel composites was also evaluated. Firstly, after 3 and 7 days of incubation, the hydrogel composites and cells were washed with PBS, fixed with 4 % paraformaldehyde, dehydrated, and observed using scanning electron microscopy (SEM). Furthermore, after 7 days of incubation, cell adhesion was also evaluated using confocal laser scanning microscopy (CLSM, LSM710, Zeiss, Germany) after staining the samples with FITC-phalloidin and DAPI.

## 2.5. In vitro osteogenesis-related assay

To eliminate the influence of hydrogels on staining, cell culture was performed in 12-well transwell plates (0.4 µm, Corning, USA) by seeding ~2 × 10<sup>4</sup> hBMSCs into the lower chambers and injecting 200 µL hydrogels into the upper chambers. Osteogenic medium (OM) containing 10 nM dexamethasone, 10 mM β-glycerophosphate, and 0.2 mM ascorbic acid was used to induce osteogenic differentiation of the hBMSCs. The PM and OM groups were cultured without hydrogel composites. NIR light irradiation (0.25 W/cm<sup>2</sup>, 10 min) of the HBC+5MP-BMP+NIR/HBC+Asp+5MP-BMP+NIR groups was performed on days 3, 7, and 11. After 14 days of culture, the cells were washed with PBS, fixed with 95 % cold ethanol, and stained using an alkaline phosphatase (ALP) staining kit (Beyotime, China) or 1 % alizarin red staining (ARS) solution (Sigma-Aldrich, USA) according to the manufacturer's protocol. Staining images were obtained using a scanner. ALP quantification was performed using an ALP assay kit (Beyotime, China) and normalized to the total protein concentration. For ARS quantification, 100 mM cetylpyridinium chloride was used to solubilize the stained cells, and the absorbance of the solution was measured at 562 nm.

## 2.6. In vivo experiments

A critical-size calvaria-defect model was established in SD rats (eight-week-old, male, weight 180–200 g) to evaluate the osteogenic capabilities of the hydrogels. All animal experiments were approved by the Peking University Animal Care and Use Committee and performed according to institutional animal guidelines. After general anesthesia and disinfection, a midline incision was made to expose the calvaria area by blunt dissection. Then, 5 mm trephine bur with low-speed drilling was used to prepare a bilateral bone defect under irrigation with 0.9 % saline solution. Then, the hydrogel was injected into the defect area and the incision was closed in layers. On day 3, 7, and 11 after hydrogel implantation, the defects for the NIR light-treatment groups were irradiated under NIR laser (0.25 W/cm<sup>2</sup>, 10 min). The local temperature of the hydrogel composite was recorded with an infrared thermal camera and maintained at ~45 °C.

## 2.7. Analysis of inflammatory response in vivo

Randomly selected rats (*n* = 3) from the PBS (blank), HBC, HBC+Asp, HBC+5MP-BMP, and HBC+Asp+5MP-BMP groups were sacrificed 48 h after surgery by CO<sub>2</sub> inhalation and the calvaria samples were harvested, fixed, decalcified, embedded, and cut into 5-µm thick sections for tartrate-resistant acid phosphatase (TRAP) staining. Meanwhile, immunohistochemistry (IHC) staining against COX2, MMP9, and CD11b (Abcam, UK) was also conducted and 3,3'-diaminobenzidine was used to develop positive staining.

## 2.8. Analysis of bone regeneration in vivo

Eight weeks after surgery, randomly selected rats (*n* = 6) from the groups treated with PBS (blank), HBC hydrogel, HBC+Asp hydrogel, HBC+5MP-BMP hydrogel with NIR light irradiation, and HBC+Asp+5MP-BMP hydrogel with or without NIR light irradiation, were sacrificed. Calvaria samples were collected and fixed for micro-CT (Siemens, Germany) scanning. Inveon research workplace software was used for 3D reconstructions. Bone mineral density (BMD, g/cm<sup>3</sup>), bone volume fraction (bone volume/tissue volume; BV/TV, %), trabecular thickness (Tb.Th, mm), and trabecular number (Tb.N, 1/mm) were used for quantification of newly-formed bone tissues. Thereafter, the samples were decalcified, dehydrated, embedded, and cut into 5-µm sections for hematoxylin & eosin (HE) staining, Masson staining, and IHC staining targeting osteocalcin (OCN), osteopontin (OPN), and Collagen Type I (COL1).

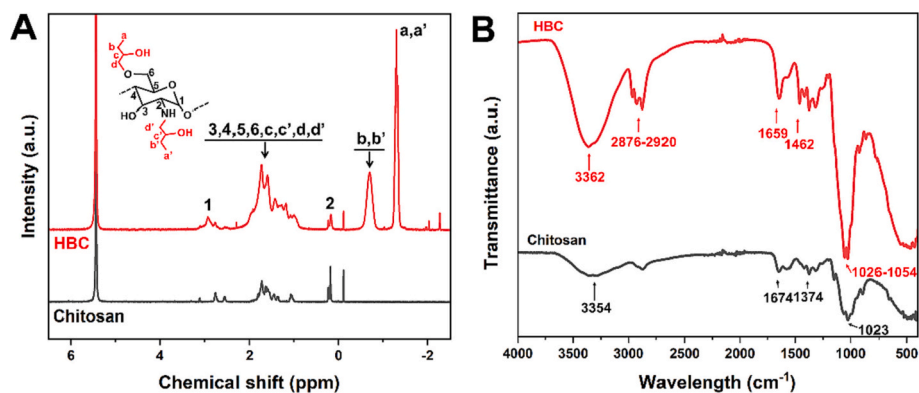


Fig. 2. (A)  $^1\text{H}$  NMR and (B) FTIR spectra of HBC and chitosan.

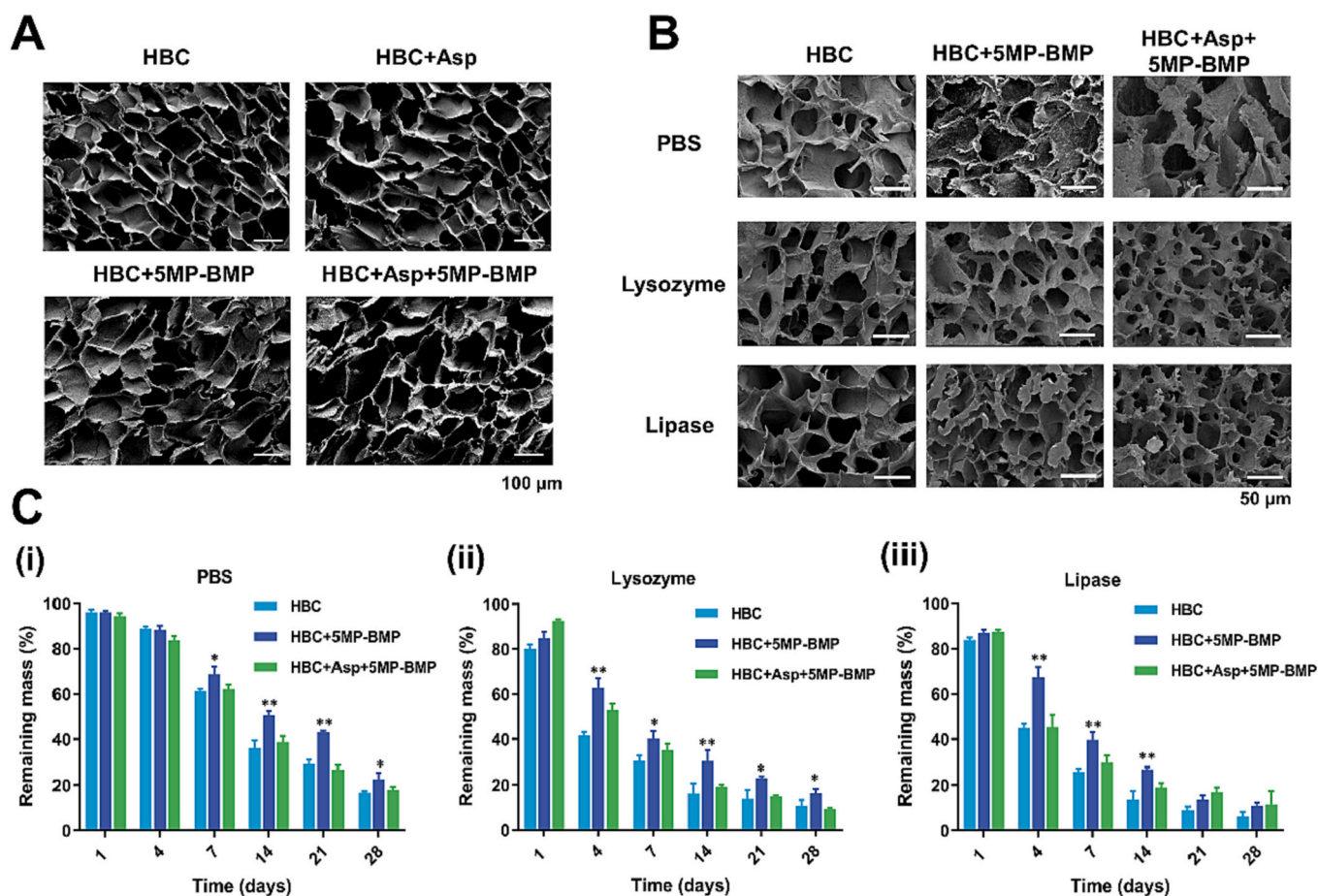


Fig. 3. (A) SEM images of freeze-dried HBC, HBC+Asp, HBC+5MP-BMP, and HBC+Asp+5MP-BMP hydrogel composites. (B) SEM images and (C) degradation rates of hydrogel composites in PBS, lysozyme, and lipase degradation solutions on day 7 ( $n = 3$  per group,  $*P < 0.05$ ,  $**P < 0.01$ ).

## 2.9. Statistical analysis

All data are expressed as mean  $\pm$  standard deviation (SD). Statistical analysis was performed by one-way analysis of variance (ANOVA) with post-hoc tests using GraphPad Prism 9 software.  $P < 0.05$  was considered statistically significant.  $*P < 0.05$ ,  $**P < 0.01$ .

## 3. Results

### 3.1. Characterization of HBC

HBC was synthesized by conjugating the ring-opening product of 1,2-

butane oxidation onto the chitosan chain. The degree of hydroxybutyl substitution was calculated to be 1.60 according to the results of elemental analysis (Table S3). The  $^1\text{H}$  NMR spectra of HBC and chitosan dissolved in 20 % DCl are presented in Fig. 2A. The solvent signal is observed at 5.4 ppm and does not obscure any characteristic peaks. New peaks for HBC at 0.8 and 1.3 ppm are assigned to the  $-\text{CH}_2-$  and  $-\text{CH}_3$  protons in the hydroxybutyl moiety, respectively. The integrated area of these two peaks corresponds to the number of hydroxybutyl protons.

The FTIR spectrum of HBC presents obvious absorption peaks around 1462 and 2876–2920  $\text{cm}^{-1}$ . These are assigned to the  $-\text{CH}_3$  bending and C–H stretching of the hydroxybutyl moiety, respectively (Fig. 2B). The absorption peak due to the C–O stretching vibration of the C6–OH

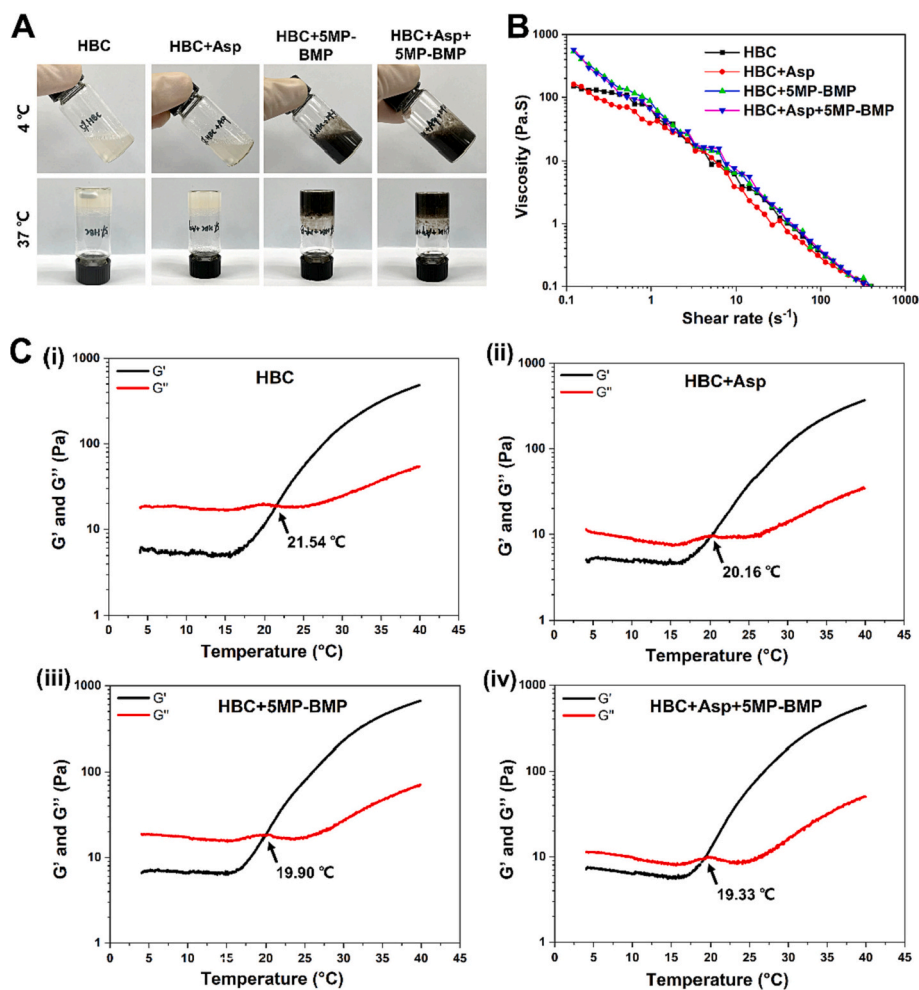


**Fig. 4.** (A) Photographs showing the initial hydrogel solutions and the resulting gels after incubation at 37 °C for 3 min. (B) Shear-rate-dependent viscosity for different hydrogel composites at 37 °C. (C) Rheological analysis results for (i) HBC, (ii) HBC+Asp, (iii) HBC+5MP-BMP, and (iv) HBC+Asp+5MP-BMP hydrogel composites.

group shifts from 1023 cm<sup>-1</sup> for chitosan to 1026–1054 cm<sup>-1</sup> for HBC, indicating that the hydroxybutyl group was successfully introduced to the C6–OH position.

### 3.2. Morphology of the hydrogel-microsphere composites

The compositions of the hydrogel composites were optimized to maintain their thermo-responsive abilities under physiological temperature (Table S2). The hydrogel composites form hydrophobic interaction domains surrounded by water molecules at 37 °C through the agglomeration of hydrophobic hydroxybutyl chains. Then, the lyophilized hydrogels were used for SEM observation (Fig. 3A). This process involves the evacuation of water molecules and consequent deswelling, generating a porous microstructure (Xu et al., 2019).

The SEM images show that the pore size of the lyophilized hydrogel composites is relatively uniform and lie in the range of 50–100 μm. In comparison with the HBC hydrogel, the incorporation of Asp and microspheres does not significantly change the pore structure of the gels, and the pore walls of the HBC+5MP-BMP and HBC+Asp+5MP-BMP hydrogels are embedded with grains.

### 3.3. Degradation and swelling behaviors of hydrogel composites

In general, the degradation of hydrogel composites proceeds with time (Fig. 3C). The HBC+5MP-BMP hydrogel exhibits slower degradation kinetics than the HBC hydrogel, and the incorporation of Asp

slightly increases the degradation rate of the hydrogel. Approximately 80 % of the hydrogels are degraded after incubation in PBS for 28 days. The degradation of the hydrogel composites is accelerated by the addition of lysozyme or lipase, resulting in ~90 % degradation after 28 days.

The SEM images of the degraded hydrogel composites taken on day 7 show that the porous structure is maintained without obvious erosion, providing a stable microenvironment for cellular migration in the early stage of bone healing (Fig. 3B). These results demonstrate the appropriate biodegradability and early stability of our hydrogel composites, both of which are essential for their *in vivo* application.

In our swelling test, the crosslinked hydrogels could gradually reach the saturated states in PBS solution at the beginning of the test (Fig. S4). Subsequently, the swelling ratio decreases with the diffusion of sol fraction in networks and the degradation of the samples.

### 3.4. Rheological characteristics

As shown in Fig. 4A, the hydrogel composites darken upon the incorporation of PDA-coated microspheres, and gelation of the hydrogels occurs upon incubation at 37 °C. Compared with the pure HBC hydrogel, the presence of Asp and microspheres reduces the gelation time (Table S2). The curves in Fig. 4C show that incipient gelation temperature (T<sub>i</sub>) for the HBC hydrogel is 21.54 °C, while T<sub>i</sub> for the HBC+Asp, HBC+5MP-BMP, and HBC+Asp+5MP-BMP hydrogels are lower. The gap between the storage modulus (G') and loss modulus (G'')

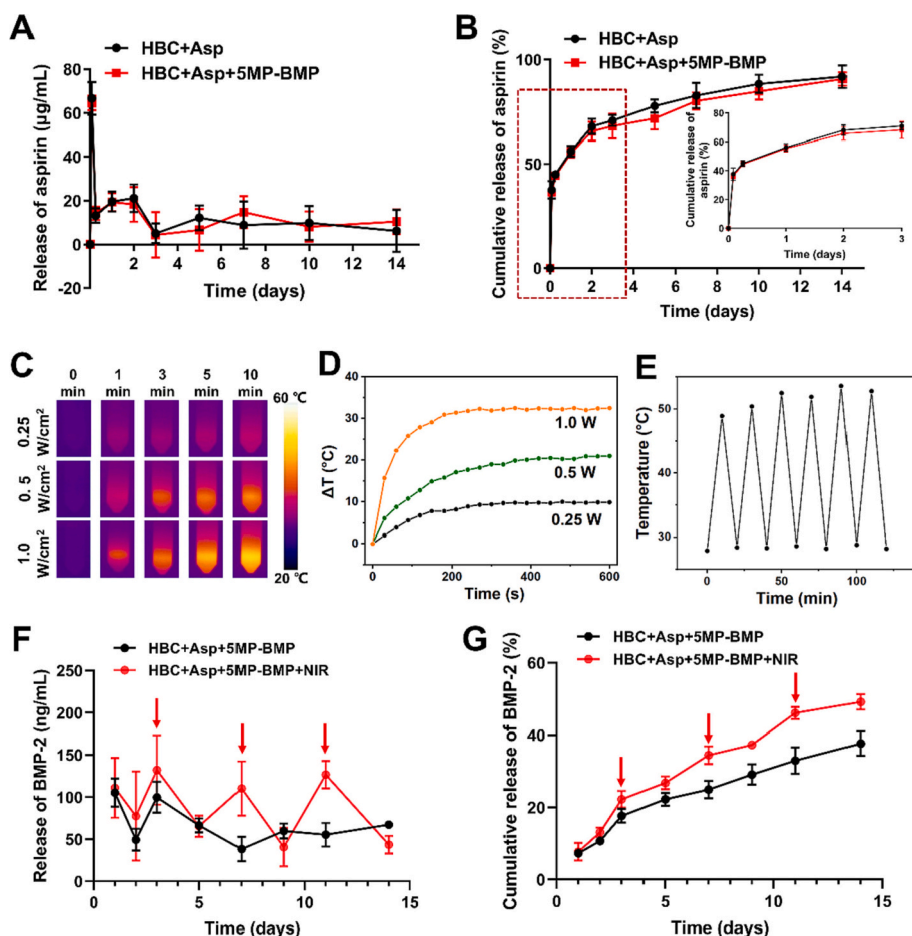


**Fig. 5.** (A) Release concentrations and (B) cumulative release of Asp from HBC+Asp and HBC+Asp+5MP-BMP hydrogels. (C) Infrared thermal images and (D) temperature changes for the HBC+Asp+5MP-BMP hydrogel under NIR light irradiation at different densities. (E) Temperature profile of the HBC+Asp+5MP-BMP hydrogel under NIR light irradiation over six cycles (808 nm, 0.25 W/cm<sup>2</sup>, 10 min on, 10 min off). (F) Release concentrations and (G) cumulative release of BMP-2 from the HBC+Asp+5MP-BMP hydrogel with and without NIR irradiation.

curves is smaller for the Asp-containing hydrogels than for the other hydrogels, indicating that the incorporation of Asp increases viscoelasticity. Furthermore, a sharply decreasing viscosity with increasing shear rate at 37 °C is observed in all samples (Fig. 4B), demonstrating their shear-thinning behavior.

### 3.5. *In vitro* Asp release

In order to exert the anti-inflammatory therapeutic effect of Asp, it was loaded into the hydrogel composites at 200 µg/mL, as based on previous studies (Liu et al., 2015; Xu et al., 2016). As shown in Fig. 5A,B, both HBC+Asp and HBC+Asp+5MP-BMP hydrogels present burst release of Asp for the first 48 h, during which the cumulative release of Asp reaches 68.04 % and 65.72 %, respectively. From day 2 to 14, Asp is continuously released at a significantly slower rate, and the release curves gradually plateau. At the end of day 14, the cumulative releases of Asp from the HBC+Asp and HBC+Asp+5MP-BMP hydrogels are 91.87 % and 90.73 %, respectively.

### 3.6. *In vitro* photothermal properties and release of BMP-2

Upon NIR light irradiation at different densities (0.25, 0.50, and 1.00 W/cm<sup>2</sup>) for 10 min, the temperature increases for the HBC+Asp+5MP-BMP hydrogel are 9.9, 20.6, and 32.5 °C, respectively (Fig. 5C). No obvious difference in maximum temperature is observed for the HBC+Asp+5MP-BMP hydrogel over six irradiation cycles (Fig. 5E), demonstrating the excellent photothermal stability of the hydrogel composite. Considering the fact that normal tissue damage caused by overheating occurs above 50 °C, an NIR light density of 0.25 W/cm<sup>2</sup> was applied for all following experiments.

The encapsulation efficiency of BMP-2 by 5MP-BMP was calculated to be  $72.01 \pm 8.96$  %, and the total loading capacity of the microspheres was calculated to be 144 ng BMP-2 per mg microspheres. Then, the BMP-2 release profile from HBC+Asp+5MP-BMP hydrogel was evaluated (Fig. 5F, G). A slight burst release of BMP-2 (around 7.5 %) is firstly observed on day 1. In the group with NIR irradiation, a significantly increased release of BMP-2 is observed at day 3, 7, and 11, and the total release of BMP-2 reaches  $49.16 \pm 2.09$  % at day 14, which maintains an optimal therapeutic concentration of BMP-2 (around 100 ng/mL). In contrast, the HBC+Asp+5MP-BMP hydrogel without NIR irradiation exhibits sustained release kinetics, with the total release of BMP-2 reaching  $37.66 \pm 3.39$  % at 14 days.

### 3.7. *In vitro* biocompatibility and osteogenic assessment

First, the 5-wt%-magnesium-containing calcium carbonate microspheres (5MCMs) with the highest osteogenic potential were utilized to prepare our hydrogel composites (Fig. S2). ALP staining confirmed the osteo-inductive capabilities of the 5MCMs, PDA-coated 5MCMs (5MPs), and 5MP-BMP (Fig. 6A). Then, CCK-8 assays showed that there is no significant difference in the cellular proliferation of hBMMSCs between each group (Fig. 6B). The confocal and SEM images (Figs. 6B and S5) show that hBMMSCs adhere well onto the surfaces of the hydrogels and exhibit a typical polygon shape with multiple filopodia, indicating that the low-density NIR irradiation as well as the incorporation of Asp and microspheres does not influence the biocompatibility of the hydrogels.

Furthermore, the results of ALP staining (Fig. 6D) show that the HBC+Asp+5MP-BMP are significantly stained after 14 days of culturing. Specifically, denser ALP staining is observed for the NIR-irradiation group. Similarly, ARS staining after culturing for 14 days reveals that

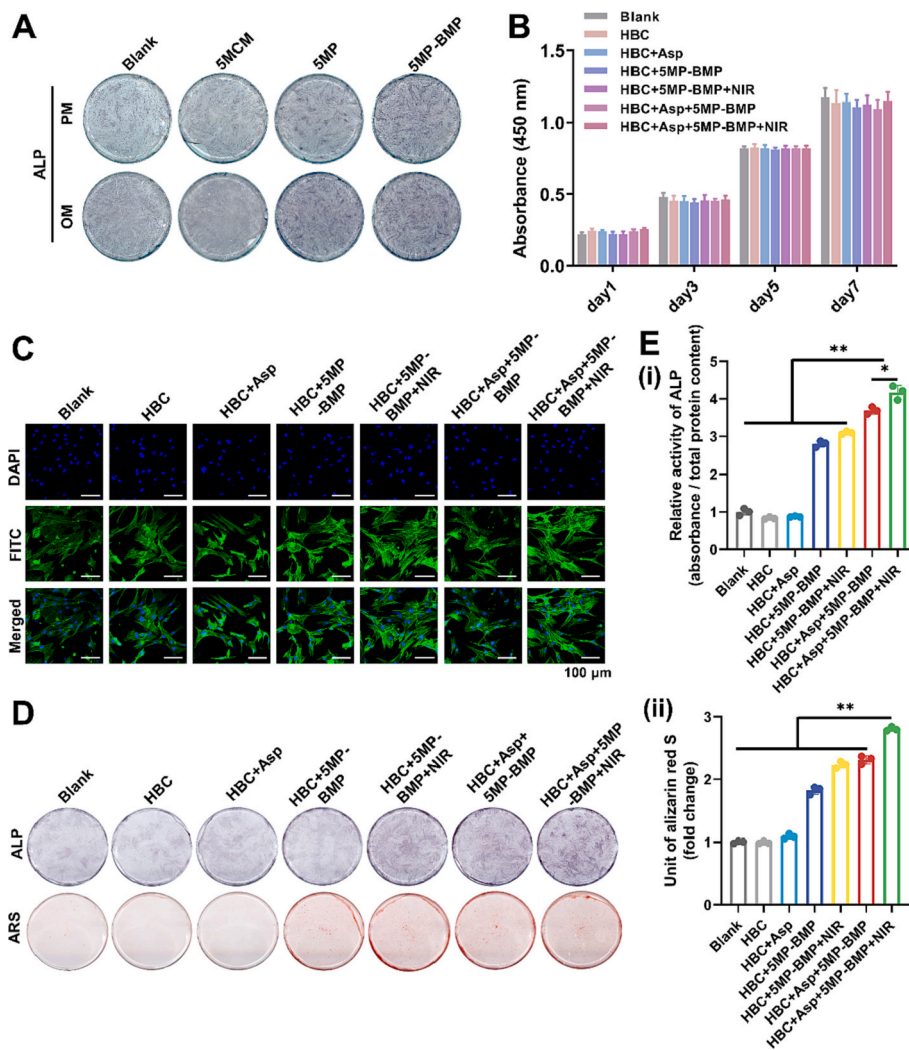


**Fig. 6.** (A) ALP staining of hBMMSCs cultured with different microspheres for 14 days. (B) Proliferation of hBMMSCs on different hydrogel composites according to CCK-8 assay. (C) Attachment of hBMMSCs to hydrogel composites as observed by CLSM. (D) ALP/ARS staining and (E) quantification of hBMMSCs cocultured with different hydrogel composites for 14 days.

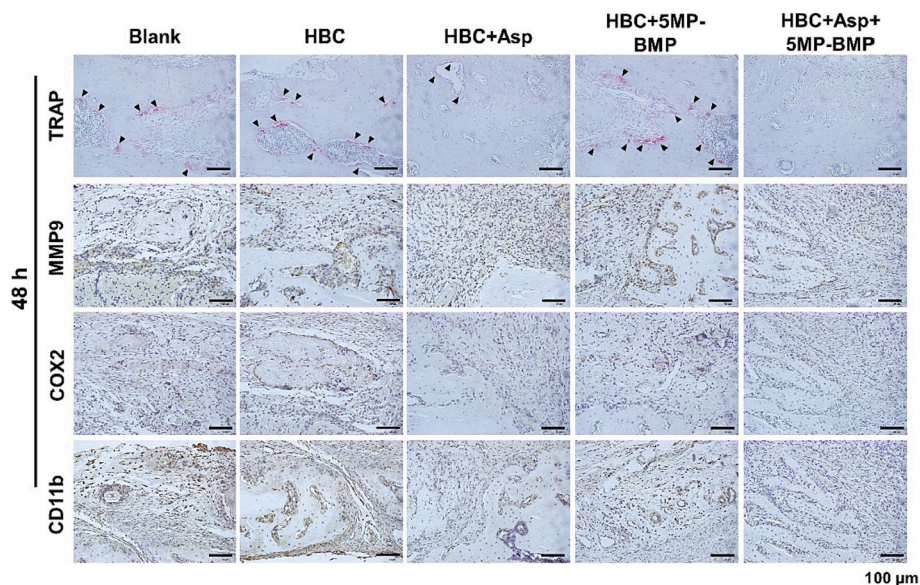


**Fig. 7.** Anti-inflammation effects of hydrogel composites *in vivo*. TRAP staining and IHC staining of MMP9, COX2, and CD11b around calvaria-defect areas 48 h after hydrogel implantation. Arrows indicate TRAP-positive cells.

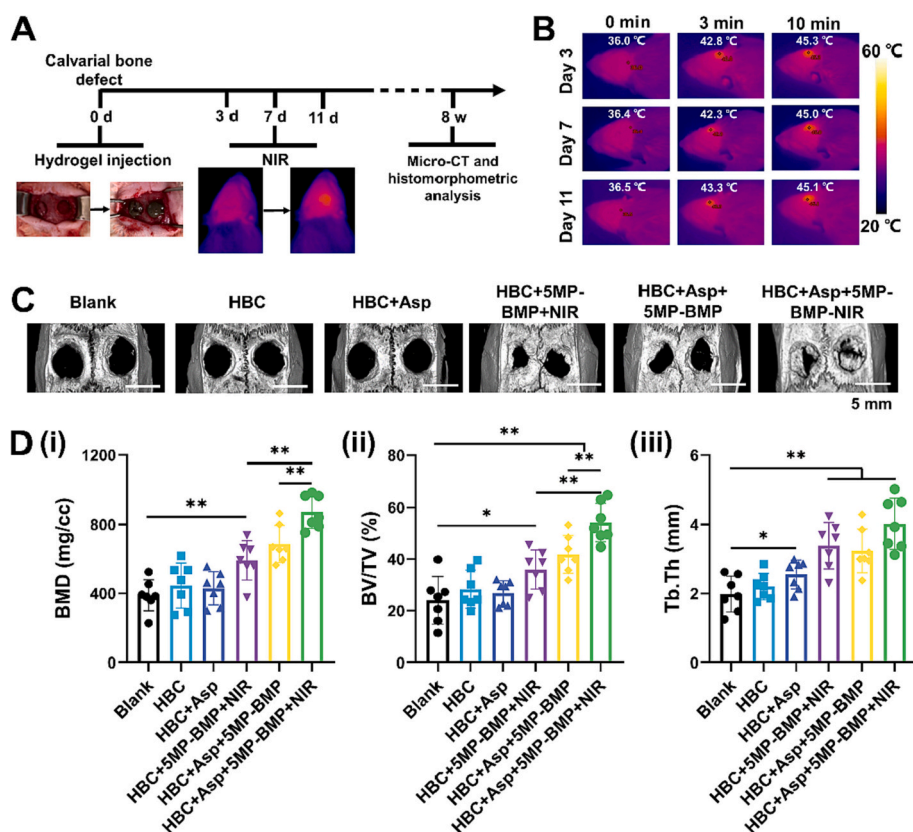


**Fig. 8.** Evaluation of the osteogenesis capabilities of the hydrogel composites *in vivo*. (A) Schematic of the *in vivo* study timeline. (B) IR thermal images of calvaria defect areas implanted with HBC+Asp+5MP-BMP hydrogel with NIR light irradiation (0.25 W/cm<sup>2</sup>, 10 min). (C) Micro-CT reconstruction images of calvarias repaired with different hydrogel composites. (D) Quantitative comparison of BMD, BV/TV, and Tb.Th between different groups (\**P* < 0.05, \*\**P* < 0.01).

the HBC+Asp+5MP-BMP+NIR group also exhibits much denser mineral nodules and a higher degree of mineralization than the control. ALP and ARS quantification results present similar trends (Fig. 6E).

### 3.8. *In vivo* inflammatory response

Local inflammatory reactions around bone defect areas were evaluated using TRAP and IHC staining 48 h after hydrogel injection (Fig. 7). The Asp-treatment groups exhibit observable fewer TRAP-positive osteoclasts than the other groups. In IHC staining, MMP9-, COX2-, and CD11b-positive cells are observed around the defect areas in the blank group. However, the Asp-containing hydrogel groups exhibit fewer MMP9-, COX2-, and CD11b-positive cells than the other groups, indicating that Asp efficiently eliminates undesirable inflammatory reaction at the early stage of bone healing.

### 3.9. *In vivo* bone regeneration

Firstly, the IR thermal images of SD rats from the HBC+Asp+5MP-BMP+NIR group (Fig. 8B) demonstrate its efficient *in vivo* photothermal conversion ability. The local temperature of the calvaria tissues was maintained around 45 °C to avoid overheating.

Then, the osteogenesis capability of the NIR-light-responsive hydrogel was evaluated. The micro-CT results demonstrate that the HBC+5MP-BMP group with NIR light irradiation reaches maximum new-bone formation more quickly than the other groups, *i.e.*, eight weeks after hydrogel injection, indicating that NIR-light-enhanced release of BMP-2 is therapeutically favorable (Fig. S6).

Thereafter, the *in situ* new-bone formation ability of hydrogel composites with sequential delivery of Asp and BMP-2 was examined. As shown in Fig. 8C, the HBC+Asp+5MP-BMP+NIR group exhibits the

highest level of new-bone formation, while obvious cavities remain for the Blank, HBC, and HBC+Asp groups.

Further quantitative analysis indicated that the BV/TV value of the HBC+Asp+5MP-BMP+NIR group is significantly elevated to 55.20 % compared with the blank group (24.10 %), the Asp-releasing HBC+Asp group (28.09 %), and the NIR-light-controllable BMP-2-releasing HBC+5MP-BMP+NIR group (39.86 %). The BMD value for the HBC+Asp+5MP-BMP+NIR group (850.78 mg/cc) is also higher than those of the other groups, indicating that the synergistic effects of Asp and BMP-2 promote bone regeneration.

Histological observation supported the results of micro-CT analyses (Fig. 9). The HE and Masson staining images show that more new-bone formation is observed for the HBC+Asp+5MP-BMP+NIR group compared with the other groups and that the hydrogels almost completely disappear from the defect areas. IHC staining also shows that more dark-brown granules are observed for the HBC+Asp+5MP-BMP+NIR group, demonstrating the significant enhancement of OCN, OPN, and COL1 expression. Furthermore, histological evaluations of the heart, liver, spleen, and kidney tissues eight weeks after hydrogel implantation revealed no obvious pathological changes for all the experimental groups (Fig. S7), indicating the excellent biocompatibility of the hydrogel composites.

## 4. Discussion

Natural bone-defect healing proceeds with a cascade of biological events including early hemostasis and acute inflammatory response, mineralization, and bone remodeling (Masters et al., 2022). Although many studies have demonstrated that co-delivery of multiple kinds of biomolecules by scaffolds efficiently enhances the process of bone regeneration, ambiguous and uncontrollable biomolecule release are

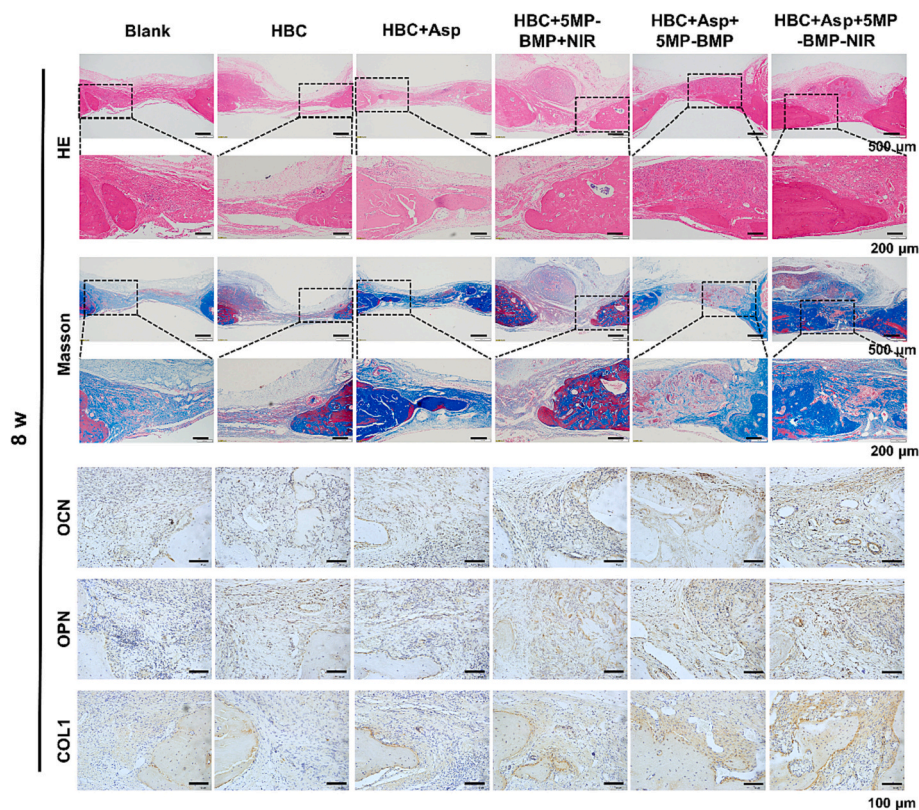


**Fig. 9.** Histological assessment of newly formed bone tissue in defect areas by HE staining, Masson staining, and IHC staining of the osteoblastic markers OCN, OPN, and COL1 eight weeks after hydrogel implantation.

obstacles to their further applications. Accordingly, we have developed a new strategy to modulate bone healing by designing a dual-responsive HBC+Asp+5MP-BMP hydrogel composite that provides sequential release of the anti-inflammatory drug Asp and the osteogenic growth factor BMP-2. The on-demand release of these clinically common biomolecules accurately regulates the early-stage inflammatory reaction as well as bone remodeling during the later stage of bone defect repair.

Hydrogels show great potential to establish extracellular-matrix-like microenvironments for cell proliferation and differentiation, and they demonstrate enormous utility as delivery vehicles for controllable drug release (Mu et al., 2020). Furthermore, flexible hydrogels can fill complex cavities *in vivo* and adapt well to defect margins, making them especially suitable for the minimally invasive repair of bone defects (Chen et al., 2021; Xu et al., 2019). In the present study, our thermo-responsive hydrogel composite exhibited feasible injectability and typical shear-thinning behavior, facilitating its application for the repair of irregular-shaped bone defects.

During the acute inflammatory stage (peaking at day 1–3) of bone healing, the tissue regeneration process is accompanied with a shifting of local inflammatory cells from pro-inflammatory toward pro-repair phenotypes (Newman et al., 2021; Zhang et al., 2021). Asp is a classical non-steroidal anti-inflammatory drug that is not subject to antibiotic resistance and inhibits the activity of cyclooxygenase, consequently reducing the production of inflammatory prostaglandin E<sub>2</sub> (Shi et al., 2020; Xu et al., 2016; Xu et al., 2019). In order to diminish undesirable inflammatory reactions and accelerate regenerative transformation of damaged bone tissues, the thermo-responsive HBC hydrogel was used as a reservoir for Asp and osteogenic microspheres in this study. According to our results, the rapid release of Asp (>60 % of the total loaded amount) from HBC hydrogel was observed within the initial 48 h owing to the small molecular structure and hydrophilicity of Asp (Fig. 5). IHC staining further confirmed that Asp-releasing hydrogels perform better *in vivo* anti-osteoclastic and anti-inflammatory functions

than those without Asp loading (Fig. 7).

Furthermore, it has been reported that the late inflammatory phase that precedes the tissue regenerative stage is the optimal therapeutic window for the delivery of osteoinductive biomolecules (Einhorn & Gerstenfeld, 2015). BMP-2 is one of the main osteoinductive growth factors reported for clinical use (Moncal et al., 2022; Salazar et al., 2016). Several studies have demonstrated that the slow and sustained release of BMP-2 successfully enhances bone regeneration (Chen et al., 2021; Chen et al., 2022). However, a long-term issue restricting the widespread application of BMP-2 is the need for supraphysiological doses (usually at the milligram level) to achieve an efficient therapeutic effect, resulting in concerns regarding safety and efficacy (Simpson et al., 2020). Thus, the design of a highly efficient BMP-2 delivery system that provides a therapeutic concentration in the appropriate bio-window within the late inflammatory stage of bone regeneration is highly desired.

In this study, NIR-responsive PDA-coated microspheres were used as a controllable-release carrier for BMP-2. It has been reported that the abundant functional groups, such as catechol, on PDA coatings act as efficient anchors for various kinds of biomolecules *via* electrostatic absorption,  $\pi$ - $\pi$  interactions, and hydrogen bonding (Cheng et al., 2019; Meng et al., 2018). Furthermore, these PDA-modified biomaterials enable the conversion of NIR light energy into heat energy, therefore providing beneficial photothermal activity as well as NIR-light-controllable biomolecule release (Gao et al., 2019; Liu et al., 2018; Xue et al., 2020). Our previous work has successfully fabricated NIR-light-responsive PDA-coated nanoparticles to allow the on-demand release of a small-molecule osteogenic drug (Wan et al., 2022). In the present study, we have extended the application of PDA-coated microspheres to control the release timeframe of BMP-2. First, our results confirmed the desirable photothermal effects of 5MP-BMP, and the release of BMP-2 was obviously increased upon NIR light irradiation (Fig. 5). NIR light irradiation was applied at days 3, 7, and 11 to increase

the concentration of BMP-2 to within a physiological range and maximize its therapeutic effects during the late inflammatory stage of bone healing. Furthermore, magnesiumcalcium carbonate microspheres with ideal osteogenic potential were chosen to prepare hydrogel composites (Fig. S2). The sustained release of  $\text{Ca}^{2+}$  and  $\text{Mg}^{2+}$  with the biodegradation of the microspheres promotes long-term bone regeneration, as previously reported (Chen et al., 2019; Douglas et al., 2016; Lopez-Heredia et al., 2018).

Our *in vivo* experiments further confirmed that NIR-light-controllable release of BMP-2 favors new-bone formation (Fig. S6). Here, the HBCAsp+5MP-BMP hydrogel composite with NIR light irradiation provided the best osteogenic capability (Figs. 8 and 9). This hydrogel composite allows the deliberate sequential release of Asp and BMP-2, playing critical roles in regulating the process of bone healing and efficiently promoting bone regeneration.

## 5. Conclusions

In this study, a dual-responsive HBC+Asp+5MP-BMP hydrogel composite with sequential release capability, in which the rapid release of Asp mitigates the acute inflammatory reaction in the early stage of bone healing and NIR-light-controllable release of BMP-2 maximizes its therapeutic effect in bone regeneration, was designed and demonstrated. This sequential release behavior cooperates well with the cascaded processes of bone healing, thereby achieving promoted bone regeneration. Moreover, this hydrogel composite may also be utilized to deliver other biomolecules in a sequential and controllable manner, providing new therapeutic strategies for the treatment of bone-related cancers and infections.

## CRedit authorship contribution statement

Zhuqing Wan: Investigation, Methodology, Data analyze, Writing-original draft; Qinyuan Dong, Xiaodong Guo, & Xiaoqiang Bai: Assisted the experiments and analysis; Xiao Zhang, Ping Zhang, & Yunsong Liu: Discussed and modified the manuscript; Longwei Lv & Yongsheng Zhou: Conceptualization, Supervision, Funding acquisition, Writing-review and editing.

## Declaration of competing interest

The authors declare that they have no known competing financial interests or personal relationships that could have appeared to influence the work reported in this paper.

## Data availability

Data will be made available on request.

## Acknowledgements

This study was supported by grants from the National Natural Science Foundation of China (81930026); Beijing Natural Science Foundation (7192228), China Postdoctoral Science Foundation (2022M710254), and the Young Elite Scientist Sponsorship Program by CAST (2015QNRC001).

## Appendix A. Supplementary data

Supplementary data to this article can be found online at <https://doi.org/10.1016/j.carbpol.2022.120027>.

## References

- Annamalai, R. T., Turner, P. A., Carson, W. F., Levi, B., Kunkel, S., & Stegmann, J. P. (2018). Harnessing macrophage-mediated degradation of gelatin microspheres for spatiotemporal control of BMP2 release. *Biomaterials*, *161*, 216–227.
- Bi, S., Kong, M., Cheng, X., & Chen, X. (2021). Temperature sensitive self-assembling hydroxybutyl chitosan nanoparticles with cationic enhancement effect for multi-functional applications. *Carbohydrate Polymers*, *254*, Article 117199.
- Chen, J., Zhou, X., Sun, W., Zhang, Z., Teng, W., Wang, F., & Li, W. (2022). Vascular derived ECM improves therapeutic index of BMP-2 and drives vascularized bone regeneration. *Small*, *2107991*, 1–16.
- Chen, S., Shi, Y., Zhang, X., & Ma, J. (2019). Biomimetic synthesis of mg-substituted hydroxyapatite nanocomposites and three-dimensional printing of composite scaffolds for bone regeneration. *Journal of Biomedical Materials Research Part A*, *107* (11), 2512–2521.
- Chen, X., Tan, B., Bao, Z., Wang, S., Tang, R., Wang, Z., & Peng, S. (2021). Enhanced bone regeneration via spatiotemporal and controlled delivery of a genetically engineered BMP-2 in a composite hydrogel. *Biomaterials*, *277*, Article 121117.
- Cheng, W., Zeng, X., Chen, H., Li, Z., Zeng, W., Mei, L., & Zhao, Y. (2019). Versatile polydopamine platforms: Synthesis and promising applications for surface modification and advanced nanomedicine. *ACS Nano*, *13*(8), 8537–8565.
- Claes, L., Recknagel, S., & Ignatius, A. (2012). Fracture healing under healthy and inflammatory conditions. *Nature Reviews Rheumatology*, *8*(3), 133–143.
- Cui, L., Zhang, J., Zou, J., Yang, X., Guo, H., Tian, H., Zhang, P., Wang, Y., Zhang, N., Zhuang, X., Li, Z., Ding, J., & Chen, X. (2020). Electroactive composite scaffold with locally expressed osteoinductive factor for synergistic bone repair upon electrical stimulation. *Biomaterials*, *230*, Article 119617.
- Douglas, T. E., Lapa, A., Reczynska, K., Krok-Borkowicz, M., Pietryga, K., Samal, S. K., & Skirtach, A. G. (2016). Novel injectable, self-gelling hydrogel-microparticle composites for bone regeneration consisting of gellan gum and calcium and magnesium carbonate microparticles. *Biomedical Materials*, *11*(6), Article 065011.
- Einhorn, T. A., & Gerstenfeld, L. C. (2015). Fracture healing: Mechanisms and interventions. *Nature Reviews Rheumatology*, *11*(1), 45–54.
- Gao, G., Jiang, Y., Jia, H., & Wu, F. (2019). Near-infrared light-controllable on-demand antibiotics release using thermo-sensitive hydrogel-based drug reservoir for combating bacterial infection. *Biomaterials*, *188*, 83–95.
- Italiani, P., & Boraschi, D. (2014). From monocytes to M1/M2 macrophages: Phenotypic vs. functional differentiation. *Frontiers in Immunology*, *5*, 514.
- Jalili, N. A., Muscarello, M., & Gaharwar, A. K. (2016). Nanoengineered thermoresponsive magnetic hydrogels for biomedical applications. *Bioengineering & Translational Medicine*, *1*(3), 297–305.
- Kim, Y. H., & Tabata, Y. (2015). Dual-controlled release system of drugs for bone regeneration. *Advanced Drug Delivery Reviews*, *94*, 28–40.
- Lienemann, P. S., Vallmajo-Martin, Q., Papageorgiou, P., Blache, U., Metzger, S., Kiveliö, A. S., & Ehrbar, M. (2020). Smart hydrogels for the augmentation of bone regeneration by endogenous mesenchymal progenitor cell recruitment. *Advanced Science (Weinh)*, *7*(7), 1903395.
- Liu, H., Li, W., Liu, Y., Zhang, X., & Zhou, Y. (2015). Co-administration of aspirin and allogeneic adipose-derived stromal cells attenuates bone loss in ovariectomized rats through the anti-inflammatory and chemotactic abilities of aspirin. *Stem Cell Research & Therapy*, *6*, 200.
- Liu, Y., Sui, Y., Liu, C., Liu, C., Wu, M., Li, B., & Li, Y. (2018). A physically crosslinked polydopamine/nanocellulose hydrogel as potential versatile vehicles for drug delivery and wound healing. *Carbohydrate Polymers*, *188*, 27–36.
- Liu, Y., Yang, Z., Wang, L., Sun, L., Kim, B. Y. S., Jiang, W., & Liu, C. (2021). Spatiotemporal immunomodulation using biomimetic scaffold promotes endochondral ossification-mediated bone healing. *Advanced Science (Weinh)*, *8*(11), Article e2100143.
- Liu, Y., Ai, K., & Lu, L. (2014). Polydopamine and its derivative materials: synthesis and promising applications in energy, environmental, and biomedical fields. *Chemical Reviews*, *119*(9), 5057–5115.
- Loi, F., Cordova, L. A., Pajarinen, J., Lin, T. H., Yao, Z., & Goodman, S. B. (2016). Inflammation, fracture and bone repair. *Bone*, *86*, 119–130.
- Lopez-Heredia, M. A., Lapa, A., Reczynska, K., Pietryga, K., Balcaen, L., Mendes, A. C., & Douglas, T. E. L. (2018). Mineralization of gellan gum hydrogels with calcium and magnesium carbonates by alternate soaking in solutions of calcium/magnesium and carbonate ion solutions. *Journal of Tissue Engineering And Regenerative Medicine*, *12*(8), 1825–1834.
- Masters, E. A., Ricciardi, B. F., Bentley, K. L. M., Moriarty, T. F., Schwarz, E. M., & Muthukrishnan, G. (2022). Skeletal infections: Microbial pathogenesis, immunity and clinical management. *Nature Reviews Microbiology*, *20*(7), 385–400.
- Meng, Y., Liu, P., Zhou, W., Ding, J., & Liu, J. (2018). Bioorthogonal DNA adsorption on polydopamine nanoparticles mediated by metal coordination for highly robust sensing in serum and living cells. *ACS Nano*, *12*(9), 9070–9080.
- Moncal, K. K., Tigli Aydin, R. S., Godzik, K. P., Aciri, T. M., Heo, D. N., Rizk, E., & Ozbolat, I. T. (2022). Controlled co-delivery of pPDGF-B and pBMP-2 from intraoperatively bioprinted bone constructs improves the repair of calvarial defects in rats. *Biomaterials*, *281*, Article 121333.
- Mu, Z., Chen, K., Yuan, S., Li, Y., Huang, Y., Wang, C., Zhang, Y., Liu, W., Luo, W., Liang, P., Li, X., Song, J., Ji, P., Cheng, F., Wang, H., & Chen, T. (2020). Gelatin nanoparticle-injectable platelet-rich fibrin double network hydrogels with local adaptability and bioactivity for enhanced osteogenesis. *Advanced Healthcare Materials*, *9*(5), Article e1901469.
- Murray, P. J., & Wynn, T. A. (2011). Protective and pathogenic functions of macrophage subsets. *Nature Reviews Immunology*, *11*(11), 723–737.

- Newman, H., Shih, Y. V., & Varghese, S. (2021). Resolution of inflammation in bone regeneration: From understandings to therapeutic applications. *Biomaterials*, 277, Article 121114.
- Rothe, R., Hauser, S., Neuber, C., Laube, M., Schulze, S., Rammelt, S., & Pietzsch, J. (2020). Adjuvant drug-assisted bone healing: Advances and challenges in drug delivery approaches. *Pharmaceutics*, 12(5), 428.
- Salazar, V. S., Gamer, L. W., & Rosen, V. (2016). BMP signalling in skeletal development, disease and repair. *Nature Reviews Endocrinology*, 12(4), 203–221.
- Shi, M., Zhang, P., Zhao, Q., Shen, K., Qiu, Y., Xiao, Y., & Zhang, Y. (2020). Dual functional monocytes modulate bactericidal and anti-inflammation process for severe osteomyelitis treatment. *Small*, 16(4), Article e1905185.
- Simpson, C. R., Kelly, H. M., & Murphy, C. M. (2020). Synergistic use of biomaterials and licensed therapeutics to manipulate bone remodelling and promote non-union fracture repair. *Advanced Drug Delivery Reviews*, 160, 212–233.
- Sun, M., Wang, T., Pang, J., Chen, X., & Liu, Y. (2020). Hydroxybutyl chitosan centered biocomposites for potential curative applications: A critical review. *Biomacromolecules*, 21(4), 1351–1367.
- Tong, L., Liao, Q., Zhao, Y., Huang, H., Gao, A., Zhang, W., & Wang, H. (2019). Near-infrared light control of bone regeneration with biodegradable photothermal osteoimplant. *Biomaterials*, 193, 1–11.
- Wan, Z., Dong, Q., Liu, Y., Zhang, X., Zhang, P., Lv, L., & Zhou, Y. (2022). Programmed biomolecule delivery orchestrate bone tissue regeneration via MSC recruitment and epigenetic modulation. *Chemical Engineering Journal*, 438, Article 135518.
- Wan, Z., Zhang, P., Lv, L., & Zhou, Y. (2020). NIR light-assisted phototherapies for bone-related diseases and bone tissue regeneration: A systematic review. *Theranostics*, 10(25), 11837–11861.
- Xu, X., Gu, Z., Chen, X., Shi, C., Liu, C., Liu, M., & Sun, H. (2019). An injectable and thermosensitive hydrogel: Promoting periodontal regeneration by controlled-release of aspirin and erythropoietin. *Acta Biomaterialia*, 86, 235–246.
- Xu, X., Zhang, K., Zhao, L., Li, C., Bu, W., Shen, Y., & Yang, B. (2016). Aspirin-based carbon dots, a good biocompatibility of material applied for bioimaging and anti-inflammation. *ACS Applied Materials & Interfaces*, 8(48), 32706–32716.
- Xue, Y., Niu, W., Wang, M., Chen, M., Guo, Y., & Lei, B. (2020). Engineering a biodegradable multifunctional antibacterial bioactive nanosystem for enhancing tumor photothermo-chemotherapy and bone regeneration. *ACS Nano*, 14(1), 442–453.
- Zhang, B., Su, Y., Zhou, J., Zheng, Y., & Zhu, D. (2021). Toward a better regeneration through implant-mediated immunomodulation: Harnessing the immune responses. *Advanced Science (Weinh)*, 8(16), Article e2100446.
- Zhang, J., Ma, S., Liu, Z., Geng, H., Lu, X., Zhang, X., & Gao, P. (2017). Guided bone regeneration with asymmetric collagen-chitosan membranes containing aspirin-loaded chitosan nanoparticles. *International Journal of Nanomedicine*, 12, 8855–8866.
- Zhao, D., Zhu, T., Li, J., Cui, L., Zhang, Z., Zhuang, X., & Ding, J. (2020). Poly(lactic-co-glycolic acid)-based composite bone-substitute materials. *Bioactive Materials*, 6(2), 346–360.
- Zhu, T., Cui, Y., Zhang, M., Zhao, D., Liu, G., & Ding, J. (2020). Engineered three-dimensional scaffolds for enhanced bone regeneration in osteonecrosis. *Bioactive Materials*, 5(3), 584–601.
- Zhu, T., Jiang, M., Zhang, M., Cui, L., Yang, X., Wang, X., Liu, G., Ding, J., & Chen, X. (2021). Biofunctionalized composite scaffold to potentiate osteoconduction, angiogenesis, and favorable metabolic microenvironment for osteonecrosis therapy. *Bioactive Materials*, 9, 446–460.